Metalorganic vapor phase epitaxy of large size CdTe grains on mica through chemical and van der Waals interactions

Dibyajyoti Mohanty,[1,2] Zonghuan Lu,[2] Xin Sun,[2,*] Yu Xiang,[2,3] Yiping Wang,[4] Debjit Ghoshal,[5] Jian Shi,[2,4] Lei Gao,[6] Sufei Shi,[2,5] Morris Washington,[2,3] Gwo-Ching Wang,[2,3] Toh-Ming Lu,[2,3] and Ishwara Bhat[1,2]

[1]*Electrical, Computer and Systems Engineering Department, Rensselaer Polytechnic Institute, Troy, New York 12180, USA*
[2]*Center for Materials, Devices and Integrated Systems, Rensselaer Polytechnic Institute, Troy, New York 12180, USA*
[3]*Physics, Applied Physics and Astronomy Department, Rensselaer Polytechnic Institute, Troy, New York 12180, USA*
[4]*Material Science and Engineering Department, Rensselaer Polytechnic Institute, Troy, New York 12180, USA*
[5]*Chemical and Biological Engineering Department, Rensselaer Polytechnic Institute, Troy, New York 12180, USA*
[6]*Corrosion and Protection Center, Key Laboratory for Environmental Fracture (MOE), University of Science and Technology Beijing, Beijing 100083, China*

(Received 21 August 2018; published 13 November 2018)

High quality heteroepitaxy of CdTe is challenging due to lattice mismatches of CdTe with many substrates. Herein, we demonstrate the epitaxial growth of single crystalline CdTe films, in multilevel island format, on mica using metalorganic chemical vapor deposition, regardless of large in-plane lattice mismatch (∼13%) between CdTe(111) and mica(001). X-ray and electron diffractions suggest that CdTe is epitaxially aligned with mica: out-of-plane CdTe(111)//mica(001) and in-plane CdTe [$\bar{1}2\bar{1}$]//mica [010]. Full-width-at-half-maximum (FWHM) of x-ray rocking curve and FWHM of x-ray azimuthal in-plane angular dispersion of CdTe are shown to be 0.11° and 0.38°, respectively, better than most CdTe films reported. Electron backscattering diffraction shows that CdTe grains are tens of μm and, if twin boundaries are excluded, in excess of 250 μm in size. In contrast to the belief that overlayer growth on mica is purely through van der Waals interaction, our first-principle calculations uncover that van der Waals interaction only contributes to 20% of the total interfacial energy, and 80% of the interfacial energy comes from chemical interaction. We believe such a strong chemical interaction is accountable for the high-quality epitaxy. The demonstration of epitaxial growth of high-quality semiconductor on mica with a large lattice mismatch creates opportunities for flexible optoelectronic devices.

DOI: 10.1103/PhysRevMaterials.2.113402

I. INTRODUCTION

CdTe thin film is one of the leading materials used in optoelectronic devices. There has been continuous interest in growing epitaxial CdTe films on a variety of single crystalline substrates. Examples of techniques used include molecular beam epitaxy (MBE) [1–3], e-beam evaporation [4], hot wall epitaxy [5], close space sublimation [6], pulse laser deposition [7], and metalorganic chemical vapor deposition (MOCVD) [8]. Examples of single crystalline substrates include Si (a = 5.43 Å) [7], Ge (a = 5.66 Å) [6], and GaAs (a = 5.65 Å) [5]. One of the challenges in these heteroepitaxy systems is the formation of structural defects in the CdTe films (a = 6.48 Å) caused by the large interface lattice mismatch.

Recently, there has been considerable interest in growing epitaxial films on substrates through van der Waals (vdW) interactions. In contrast to conventional chemical epitaxy where sharing or transferring of electrons occurs at the film-substrate interface, van der Waals epitaxy (vdWE) is believed to be based on a physical Coulombic force through dipole interactions. Since there is no "dangling bond" at the surface under the weak vdW force, it is believed that the requirement in conventional chemical epitaxy of lattice matching may be lifted, and high quality epitaxial films can be grown even when the lattice mismatch between the film and substrate is very large. This implies that strain can be relaxed right at the interface during growth, and the growth of a high quality epilayer with its own lattice parameters is possible even from the first layer [9,10]. To date, several attempts have been made to grow CdTe on vdW substrates such as graphene. In one study, CdTe was grown on defected graphene that had been irradiated by UV to enhance the nucleation sites. The CdTe film grown on such a defected graphene was polycrystalline [11]. In addition, vdWE growth of CdTe(111) thin films on commercial polycrystalline graphene buffered SiO_2/Si substrates using MOCVD technique was demonstrated. However, the CdTe film contained multiple orientational domains (grains) [12] due to the polycrystalline nature of the commercial graphene.

An alternative vdW substrate is mica. Muscovite mica ($K_2O \cdot Al_2O_3 \cdot SiO_2$) is a layered material which has been widely studied as a template for vdWE growth. Thin layers of mica are flexible, durable, inexpensive, and can be easily cleaved from the bulk material revealing a surface that has over 1 cm^2 step-free areas [13] and is stable up to 700 °C [14]. Overlayers grown on mica can be transferred to arbitrary substrates using a bubble-based method [15], suggesting promise for flexible electronics. Previous attempt to grow CdTe film on mica has been reported by DC reactive magnetron sputtering

*Corresponding author: sunx12@rpi.edu

TABLE I. A comparison of major similarity and differences of CdTe films grown on mica at 450 °C and 250 °C by MOCVD.

Growth temperature	450 °C	250 °C
Film morphology	Triangular islands	Round islands
Film thickness	∼100 nm	∼100 nm
Lateral grain size range	Tens of μm	Sub μm to several μm
Vertical interlayer spacing d_{111}	3.74 Å	*Same as the left*
FWHM of rocking curve	$0.107 \pm 0.01^\circ$	$0.338 \pm 0.002^\circ$
FWHM of x-ray {111} poles	$0.38 \pm 0.09^\circ$	$2.65 \pm 0.12^\circ$
Epitaxial relationship	Out-of-plane: CdTe(111)//mica(001); In-plane: CdTe [$\bar{1}2\bar{1}$]//mica [010] CdTe [$10\bar{1}$]//mica [100]	*Same as the left*

[16]. However, the film was polycrystalline. Vapor transport method of ultrathin CdTe nanosheets on mica has been tried, where each nanosheet was a single crystal but the ensemble of all nanosheets was not known [17]. Nonplanar CdTe nanorods on mica was also reported using chemical vapor transport technique [9]. Each nanorod was a single crystal but, again, the ensemble of nanorods was polycrystalline.

In the present work, we demonstrate the epitaxial growth of ∼100-nm-thick planar, continuous, and single crystalline CdTe films on mica substrates using MOCVD regardless of the very large lattice mismatch of ∼13% at the interface between CdTe(111) and mica(001). X-ray diffraction (XRD) results show that the single crystalline CdTe has the epitaxial relationships with respect to mica: out-of-plane CdTe(111)// mica(001) and in-plane CdTe [$\bar{1}2\bar{1}$]//mica [010] and CdTe [$10\bar{1}$]//mica [100]. The high quality of the CdTe film is revealed from the full-width-at-half-maximum (FWHM) of the rocking curve and the FWHM of the in-plane angular dispersion that are 0.11° (=360 arcs) and 0.38°, respectively. The rocking curve from our ultrathin ∼100 nm CdTe film is a factor of three narrower than that of similar thickness CdTe(111) films grown by close space sublimation on single crystalline Ge substrate [6] but a factor of three broader than CdTe(111) films grown by hot wall epitaxy on GaAs(001) [5]. Electron backscattering diffraction (EBSD) of this film reveals a large number of twin boundaries. However, if twin boundaries are excluded, very large grain size in excess of 250 μm is observed. Results of transmission electron microscopy (TEM) cross section and planar views support the finding of epitaxial relationship from x-ray, reflection high-energy electron diffraction (RHEED) and EBSD pole figures. First-principles density functional theory (DFT) calculations show that in addition to the conventional van der Waals interaction, a stronger chemical interaction exists at the interface which contributes to ∼80% of the total interfacial energy. This may explain the small angular orientation dispersion between the film and the substrate. Our high quality single crystalline CdTe film, in multilevel island format, with very large grain size grown on mica template may lead to applications in high efficiency and flexible optoelectronic devices that are not available on rigid single crystalline substrates.

II. RESULTS AND DISCUSSION

In this work, we present the results of two CdTe films grown under similar growth conditions except the growth temperature, one at 450 °C and the other one at 250 °C. Table I lists the comparison of results from these two films. In the main text, the film grown at 450 °C is focused on. The film grown at 250 °C is mainly described in the Supplemental Material of Figs. S1 to S4 [18].

A. Surface morphology examined by AFM and SEM

The freshly cleaved mica is featureless with the vertical root mean square roughness in the sub nm regime and the lateral correlation length in the order of several tens of μm [19]. Figures 1(a) and 1(b) show the surface morphology of a ∼100-nm-thick CdTe film grown on mica at 450 °C imaged by atomic force microscopy (AFM) and scanning electron microscopy (SEM), respectively. The surface of the CdTe film shows predominantly triangular shaped pyramidal islands. The islands are multilevels with smaller islands sitting on top of larger islands. The vertical root mean square roughness extracted from the AFM image is 37.2 ± 0.01 nm. The lateral feature sizes range from sub μm to several μm. The edges of the triangular islands are well aligned with each other or having a 60° rotation with respect to each other. The smaller island on top of the larger island implies the existence of an Ehrlich–Schwoebel barrier [20–24]. It indicates that at this temperature (450 °C), after the initial nucleation the adatoms would diffuse on mica and grow toward their equilibrium shape with large surface feature sizes. The grain size determined by EBSD, to be presented later, is large, in the tens of μm. See Table I.

The triangular shaped CdTe islands were also observed by researchers in ultrathin nanosheets grown by chemical vapor transport method where two zone temperatures, 690–720 °C and 560–590 °C, were employed [17]. Those temperatures were higher than our 450 °C growth temperature. We also found that epitaxial growth can be achieved at a temperature as low as 250 °C. In contrast to the film grown at 450 °C, the morphology of film grown at 250 °C has round island shape with a smaller feature size as compared to that grown at 450 °C. A film grown at 250 °C is shown in Fig. S1 [18]. Belyaev *et al.* reported the initial stage of CdTe grown by thermal evaporation on mica at ∼230 K, where the island size exhibited a delta function distribution with the island size of 20–25 nm [25]. Our observation is consistent with their morphology and agrees with the trend of decreasing island size with the decreasing growth temperature. In their work, although there were RHEED diffraction patterns of the initial

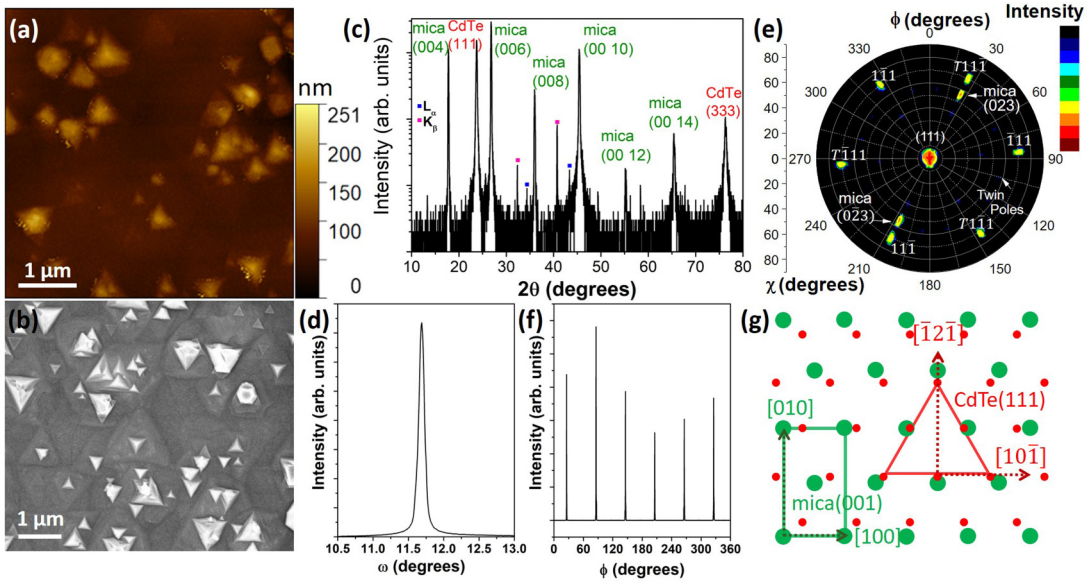

FIG. 1. (a) AFM image and (b) SEM image of the CdTe film grown on mica at 450 °C. (c) X-ray θ vs. 2θ scan. (d) X-ray rocking curve of the CdTe(111) reflection. (e) X-ray pole figure of CdTe {111} with three primary poles and three twin poles labeled. The "*T*" in (e) means twins. (f) An azimuthal scan of the six CdTe {111} x-ray poles at $\chi = 70.5°$. The adjacent poles are ~ 60° apart. (g) The real space lattice overlay of the relative epitaxial relationship between CdTe(111) (red) and mica(001) (green).

stage of CdTe growth at one azimuthal angle revealing the (111) out-of-plane orientation of CdTe, the in-plane epitaxial relationship was not reported.

B. Crystal structure and epitaxial relationship between CdTe and mica examined by XRD

Figure 1(c) shows x-ray θ *vs.* 2θ scan of the CdTe film on mica at 450 °C. Strong mica $(00l)$ peaks for $l = 2n$ with integer $n = 2$, 3, 4, 5, 6, and 7 are observed. This shows that mica is a single crystal with the (001) surface orientation. Mica has a monoclinic structure (space group *C 2/c* and number 15) with the theoretical bulk lattice constants $a = 5.225$ Å, $b = 9.163$ Å, and $c = 20.275$ Å, $\alpha = \gamma = 90°$, $\beta = 95.78°$. The interplanar spacing d_{hkl} for the (hkl) planes is given by $d_{hkl} = \{\frac{1}{\sin^2\beta}(\frac{h^2}{a^2} + \frac{k^2\sin^2\beta}{b^2} + \frac{l^2}{c} - \frac{2hl\ \cos\beta}{ac})\}^{-1/2}$. The measured lattice constant c averaged over the six mica peaks $(00l)$, where $l = 4$, 6, 8, 10, 12, and 14, is 20.07 ± 0.11 Å, slightly lower than the bulk lattice constant c.

Besides mica peaks, a strong CdTe(111) peak at $2\theta = 23.74°$ and a weak (333) peak at $2\theta = 76.31°$ are observed. The CdTe has a cubic structure (space group $F\bar{4}3m$ and number 216, $a = b = c = 6.481$ Å, and $\alpha = \beta = \gamma = 90°$). The d-spacing calculated from $2\theta = 23.74°$ is 3.74 Å which is consistent with the CdTe(111) orientation. The same result is obtained from the film grown at 250 °C as shown in Fig. S1 [18] and Table I. The vertical interlayer spacing $d_{111} = 3.74$ Å determined from both films indicate that the film is relaxed in the vertical direction, has a cubic structure with a lattice constant of 6.48 Å, and the out-of-plane orientation is (111).

Figure 1(d) shows the rocking curve when the θ is set at 11.87°. The FWHM of the rocking curve measured from the CdTe film grown at 450 °C on mica is 0.107 ± 0.001°. This is small compared to the ~0.73° FWHM of the rocking curve of the epitaxial CdTe film grown on graphene by the MOCVD technique [12]. Our 0.107° (= 385 arcs) FWHM rocking curve is narrower than ~700 arcs from ~200-nm-thick CdTe film grown by MBE on Ge(100) [3], ~1000 arcs from submicron thick CdTe film grown by close space sublimation on Ge [6], and ~14400 arcs (~ 4°) from 300-nm-thick CdTe(111) film grown by pulsed laser deposition on Si(100) [7]. Our 385 arcs is comparable to ~300 arcs from a few-μm-thick CdTe films grown by MBE on single crystalline GaAs(100) [26], wider than ~100 arcs of 1-μm-thick CdTe(111) film grown by MBE on GaAs(001) [1] or 5 or 7-μm-thick CdTe(111) films grown by MBE on GaAs(100) [1]. The film grown at 250 °C has a rocking curve FWHM of 0.338° (=1217 arcs). See Table I and Fig. S1 [18].

Since the rocking curve is an indication how parallel the (111) plane is to the mica (001) plane and does not reveal the quality of the in-plane epitaxy, the x-ray pole figure was utilized to study the in-plane alignment. Figure 1(e) shows the measured x-ray pole figure of the CdTe film grown at 450 °C by setting the 2θ at 23.74° for the {111} pole measurement. Six poles with 60° apart in the azimuth angle are observed at chi angle $\chi = 70.5°$. Theoretically, the CdTe(111) pole figure has a total of four poles, one at the center $\chi = 0°$ and three at $\chi = 70.5°$ with 120° azimuthal angle apart. The fact that there are six poles at $\chi = 70.5°$ implies there exists a second set of orientation grains which are twins of the first set of primary orientation grains. Figure 1(f) shows the azimuthal scan of the CdTe {111} poles at $\chi = 70.5°$. The average of the six FWHMs and their standard deviation of the CdTe {111} poles is 0.38 ± 0.09°. This value represents the angular spread of CdTe grains in the in-plane direction which is much smaller than angular spread of > 10° that was found in CdTe films grown on graphene [12]. The average FWHM from film grown at 250 °C is 2.65° ± 0.12° as listed in Table I.

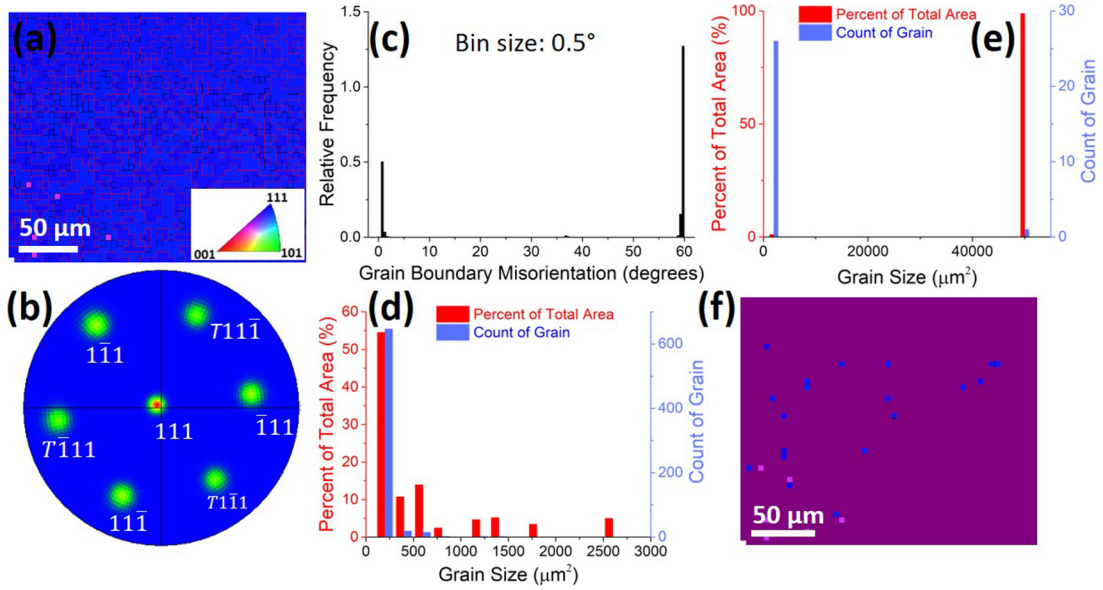

FIG. 2. (a) EBSD crystallographic orientation map (250 μm × 200 μm) of the CdTe film grown on mica at 450 °C using IPF-Z mapping component shows a uniform blue color with red curved lines indicating twin grain boundaries. (b) EBSD CdTe {111} pole figure shows three primary poles and three twin poles 60° apart. (c) Histogram of grain boundary misorientation angle distribution in the CdTe film ranging from 0° to 60°. (d) Grain size distribution (including twin grains) in the CdTe film using the grain area as the grain size parameter (bin size: 200 μm^2). (e) Grain size distribution (excluding twin grains) in the CdTe film using the grain area as the grain size parameter (bin size: 2000 μm^2). In (d) and (e), left *Y*-axis is the percentage of grain occupied area related to that specific grain size; right *Y*-axis is the count of grains related to the same specific grain size. (f) The whole EBSD IPF-Z map selected as a single crystal grain (indicated by the magenta color) if twin boundaries are excluded.

There are poles from mica in addition to the CdTe {111} poles shown in Fig. 1(e). For example, the mica (023) pole at $\chi = 56°$ is aligned with one of the CdTe {111} poles at $\chi = 70.5°$. The theoretical d spacing for mica (023) pole is 3.74 Å with the corresponding $2\theta = 23.79°$. This 2θ angle of mica (023) peak is close to the 2θ angle of CdTe(111) peak experimentally set at 23.74°. Therefore, the intensity of mica (023) pole was picked up in the pole figure measurement of the CdTe film. Another mica ($0\bar{2}3$) pole 180° azimuthally away from mica (023) was also picked up and this mica pole is aligned with one of the six CdTe {111} poles. From the pole alignment between the CdTe {111} poles and mica (023) and ($0\bar{2}3$) poles in the azimuthal direction, the in-plane epitaxial relationships are determined to be CdTe [$\bar{1}2\bar{1}$]//mica [010] and CdTe [$10\bar{1}$]//mica [100]. See Fig. 1(g). Similar result is obtained from the film grown at 250 °C. See Fig. S1 [18].

C. Grain size examined by EBSD

To further study the microstructure of this epitaxial CdTe(111) film, including the primary and twin grains, EBSD analysis was carried out. Figure 2 shows EBSD data from the CdTe film grown at 450 °C. Figure S2 shows data from the CdTe film grown at 250 °C [18]. Figure 2(a) shows the crystallographic orientation map of the CdTe film using the inverse pole figure (IPF)-Z component that correlates the spatial crystallographic orientations with respect to the normal of the sample surface. The uniform blue color in Fig. 2(a) indicates the normal direction to be ⟨111⟩ across the whole sample, consistent with the results from the XRD θ *vs*. 2θ scan and x-ray CdTe {111} pole figure measurements. The red curved lines are mainly twin grain boundaries. Figure 2(b) shows an EBSD {111} pole figure. There are six spots: three primary poles and three twin poles. This means there are two sets of orientational grains in the CdTe film, including a primary set of grains and a set of twin grains with 60° rotation in the azimuthal direction relative to the primary grains.

The twin boundaries are the coincidence site of lattice boundaries with a sigma (Σ) value of 3, indicating a 60° in-plane rotation of the crystal orientation. First-principles DFT shows that the $\Sigma 3$ grain boundary is mostly stable due to the absence of dangling bonds or wrong bonds [27]. Figure 2(c) is a histogram of grain boundary misorientation angle distribution in the CdTe film ranging from 0° to 60°. It is shown that the misorientation is dominated by the twin boundaries (60°). Figure 2(d) shows the grain size distribution (including twin grains) in the CdTe film using the grain area as the grain size parameter (bin size: 200 μm^2). The estimated diameter of these grains has a distribution up to tens of μm. For the CdTe film grown at 250 °C, the size is smaller. See Fig. S2 [18]. In Fig. 2(e), grain size distribution in the CdTe film is replotted by excluding twin boundaries and using the grain area as the grain size parameter (bin size: 2000 μm^2). It is seen that the estimated diameter of grains increases to hundreds of μm. In Figs. 2(d) and 2(e), left *Y*-axis is the percentage of grain occupied area related to that specific grain size and right *Y*-axis is the count of grains related to the same specific grain size. Figure 2(f) shows the EBSD IPF-Z mapping by excluding twin boundaries, where it is found that the whole map represents a single piece of crystal grain (indicated by the dark magenta color). It means the grain is in excess of

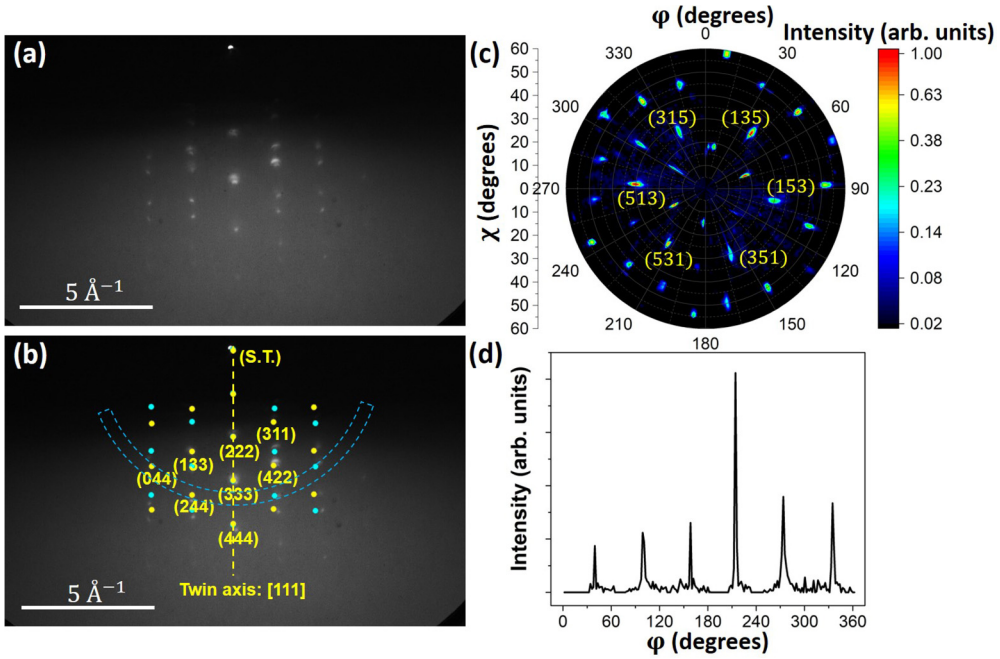

FIG. 3. (a) A RHEED pattern measured at room temperature from the CdTe film grown on mica at 450 °C using 20 keV electron energy along the [01$\bar{1}$] zone axis. (b) Calculated primary diffraction spots in yellow and twin diffraction spots in cyan. S.T. stands for the straight through spot. The vertical dashed line is the [111] twin axis. (c) The constructed RHEED pole figure with the (111) out-of-plane orientation. The χ angle ranges from 0 to 60°. Miller indices are labeled for corresponding poles. (d) An azimuthal scan of {315} poles at $\chi = 28°$.

250 μm in lateral dimension. Figure S2 shows that the film grown at 250 °C is qualitatively similar to the film grown at 450 °C if twin boundaries are excluded [18].

D. Surface structure revealed by RHEED pole figure

To study the near surface structure and symmetry of the CdTe film, we carried out a RHEED pole figure analysis [28,29] of the film grown on 450 °C. Figure 3(a) is a RHEED pattern collected at room temperature and an azimuthal angle along the [01$\bar{1}$] zone axis from the CdTe film under 20-keV incident electron energy. Sharp and symmetric diffraction spots with respect to the vertical center line going through the straight through (S.T.) spot are observed. Figure 3(b) shows a simulated pattern overlaid on the original RHEED pattern in Fig. 3(a). The yellow spots in Fig. 3(b) are the simulated diffraction spots along the [01$\bar{1}$] zone axis using the bulk lattice constant of CdTe. The Miller indices (*hkl*) are labeled below the corresponding spots. The cyan spots are the simulated twin spots of the yellow spots with the twin axis [111] outlined as the yellow dashed vertical line. The simulated diffraction pattern matches the experimental RHEED pattern very well. The RHEED pole figure obtained from a hundred RHEED patterns collected by rotating the sample with a 1.8° step size is shown and labeled in Fig. 3(c). The block between two blue dashed arcs shown in Fig. 3(b) indicates the section where the RHEED pole figure is constructed from. All poles at $\chi > 60°$ are blocked by the shadow edge.

There are many primary poles and twin poles because the *d*-spacing of these (*hkl*) planes are very close. For example, the *d*-spacings for {442}, {315}, and {440} poles are 1.08, 1.09, and 1.15 Å, respectively. An azimuthal scan of the {315} poles at $\chi = 28°$ is shown in Fig. 3(d). It reveals six poles that are evenly separated by $\sim 60°$, which is consistent with the six poles from the x-ray and EBSD pole figures. Thus, it can be concluded that the texture of this film is consistent from surface to film bulk. Similar results can be found for the film grown at 250 °C, shown in Fig. S3 [18]. Note that the average of the six FWHMs from the RHEED pole figure in Fig. 3(c) is 2.2 ± 1.0°, which is larger than the 0.38 ± 0.09° value obtained from the x-ray azimuthal scan. The observed larger FWHMs from the RHEED pole figure is partly due to the larger RHEED instrument response width [8] which mainly comes from the finite penetration depth (mean free path) of RHEED through the surface structure. The depth is < 20 nm for our 20 keV incident electron beam energy.

E. Local microstructure revealed by TEM – cross section and planar views

Figure 4(a) shows a low magnification, cross-sectional TEM image of the CdTe on mica sample grown at 450 °C. The thickness of the CdTe film is about 50 nm with some variations. The uniform contrast of the CdTe film with the absence of any grain boundary shows a good crystallinity and a sharp interface. Selected area electron diffractions (SAED) of mica and CdTe are shown in Figs. 4(b) and 4(c), respectively. The diffraction pattern of mica substrate was taken along the [1$\bar{1}$0] zone axis, showing a very dense number of diffraction spots in the (00*l*) direction, consistent with the large *d*-spacing along this direction. The diffraction pattern of CdTe, shown in Fig. 4(c), shows a pattern along the [1$\bar{1}$0] zone axis for a cubic lattice, with the (111) direction aligned with the surface normal. Figure 4(d) shows the diffraction pattern

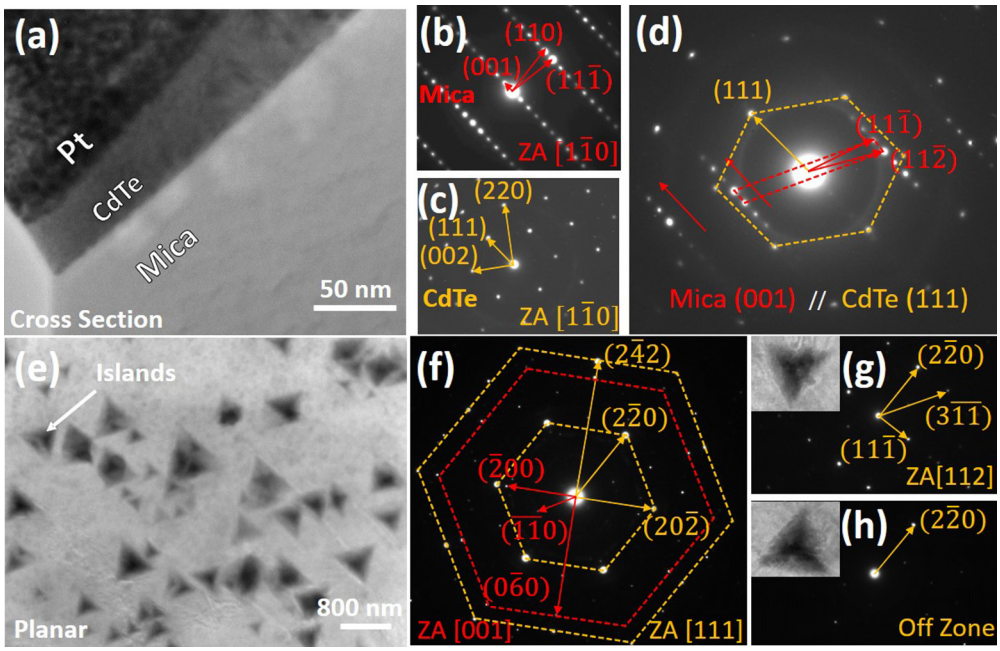

FIG. 4. TEM characterization of the CdTe film grown on mica at 450 °C. (a) Low magnification, cross-section TEM image of the CdTe/mica sample. Pt is used as a protection layer during the FIB thinning process. (b)–(c) Diffraction patterns of mica substrate and CdTe film, respectively, in the cross-section geometry. The (*hkl*) diffraction spots from mica and CdTe are indexed. The zone axis for both diffraction patterns is [1$\bar{1}$0]. (d) Diffraction pattern of the CdTe and mica interface in the cross-section geometry with the zone axis tilted along CdTe [1$\bar{1}$0]. (e) Low magnification, planar TEM image of CdTe on mica showing triangular-shaped CdTe islands. (f) Diffraction patterns of both CdTe and mica in the planar geometry. The (*hkl*) and lattices of mica (red dashed line) and CdTe (gold dashed line) have been indexed and outlined for easier visualization of the epitaxial relationship. The zone axes for mica and CdTe are [001] and [111], respectively. (g)–(h) Diffraction patterns of two CdTe triangle islands with different orientations. The pattern in (g) is obtained after tilting the sample to the [112] zone axis and the pattern in (h) is off-zone axis and the intensity becomes dimer. The insets of (g) and (h) show the morphology of the corresponding CdTe islands investigated.

of the interface containing both CdTe and mica, with the zone axis tilted to that of CdTe. The first Brillouin zone of CdTe is highlighted in gold. The (*hkl*) in the superposed patterns are labeled in red and gold for mica and CdTe in Figs. 4(b) and 4(c), respectively. It can be seen that the (111) direction of CdTe (gold arrow) and the (001) direction of mica (red arrows) point to the same direction, which agrees with the out-of-plane direction characterized by XRD.

To further study the in-plane epitaxial relation between CdTe and mica and possible twinning in the CdTe film, a planar TEM characterization was performed. Figure 4(e) shows a low magnification TEM image of the as-prepared sample over a relatively large area. Highly oriented triangular CdTe islands growing on the flat CdTe film base with two configurations (tip of island pointing upwards or downwards) can be seen, implying the epitaxial growth of the CdTe film. These triangular shape islands are consistent with that imaged by AFM and SEM shown in Figs. 1(a) and 1(b). Figure 4(f) shows the planar TEM diffraction pattern with the zone axis parallel to the sample surface normal. The two sets of diffraction pattern corresponding to the CdTe film (gold) and mica substrate (red) have been indexed by (*hkl*). The in-plane patterns for both CdTe and mica are consistent with the in-plane epitaxy relation obtained by the x-ray pole figure analysis, i.e., CdTe [$\bar{1}$2$\bar{1}$]// mica [010] and CdTe [10$\bar{1}$]// mica [100]. Note that both ($\bar{1}$2$\bar{1}$) and (10$\bar{1}$) are forbidden diffraction, so we can only observe ($\bar{2}$4$\bar{2}$) and (20$\bar{2}$) as shown in Fig. 4(f). Gold and red hexagons are used to illustrate the individual lattices for CdTe and mica, respectively. The nonoverlapping lattices show an incommensurate epitaxy and good tolerance for lattice mismatch in vdWE. We also used objective aperture to cover the (2$\bar{2}$0) diffraction spot for a dark field image to check the presence of grain boundary. However, for the entire TEM sample covering a whole mesh of 35 μm × 35 μm area, we can only see one single grain, supporting the conclusion of large grain size in the EBSD analysis.

We also attempted to characterize the microstructural difference of the CdTe twin grains revealed earlier by pole figures. Intuitively the two configurations of triangle islands (60° rotational apart) are indicative of twin. To confirm it, we picked two triangles with opposite tip pointing directions (close to each other in location), shown in the insets of Figs. 4(g) and 4(h). We tilted one of them to the zone axis of [112] with a lower symmetry. From the diffractions patterns shown in Figs. 4(g) and 4(h), the triangle island pointing downwards was tilted to the [112] zone axis to show a symmetric and bright diffraction pattern, and the pattern for the triangle island pointing upwards became dim and off the zone axis. This observation confirms that the two types of triangles are of different orientations and twin to each other.

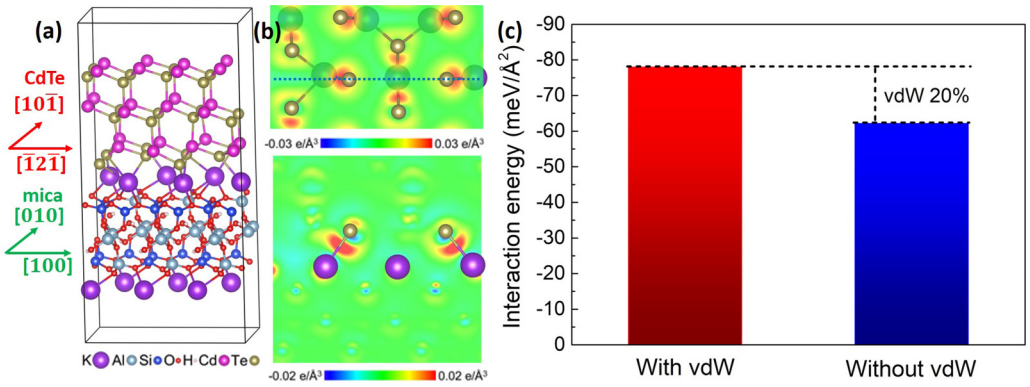

FIG. 5. DFT simulation of the interfacial interaction between CdTe and mica. (a) Atomistic model of the relaxed supercell used in DFT calculations. The atoms have been labeled and drawn to its relative sizes. The interface alignment relationship is labeled to the left of (a). (b) The upper panel is the planar view of atomic stacking and charge transfer at the CdTe/mica interface. The lower panel is the cross section noted as the blue dashed line in the upper panel, and a significant charge transfer between the K atoms layer and Te atoms layer can be observed. (c) Calculation of the interaction energy at the interface with and without vdW interaction.

F. DFT calculations of the interfacial characteristics

The DFT calculations were performed using the Vienna *ab initio* Simulation Package (VASP) [30]. The projector-augmented-wave method was utilized to model the core electrons [31]. The electron exchange and correlation were modeled within the generalized gradient approximation using the Perdew-Burke-Ernzerhof (PBE) form [32]. A nonlocal optB86b-vdW exchange-correlation functional [33,34] was used to describe the dispersion interaction (vdW forces) approximately, as it has been demonstrated to be among the most accurate vdW functional [35]. The plane wave basis kinetic energy cut off was set to 400 eV. In the simulation supercell, the mica was selected as the substrate and three layers of CdTe lattices were put on the mica surface to simulate the growth interface. The top K atoms layer of mica and the three layers CdTe lattices were allowed to relax until the forces on all the relaxed atoms were less than 0.05 eV/Å. The supercell in the calculation was constructed as following alignment relationships: out-of-plane CdTe(111)//mica(001) and in-plane CdTe [$\bar{1}$2$\bar{1}$]//mica [100] and CdTe [10$\bar{1}$]//mica [010]. Note that this alignment was 90° offset with respect to the experimental alignment. The reason for doing so was because the size of supercell would be too large to handle in VASP if the experimental alignment was chosen. But nevertheless, no matter which alignment relationship was chosen, the qualitative conclusion would hold the same.

Figure 5(a) is the relaxed mica/CdTe supercell, and we can clearly observe the existence of distortion at the interface of mica/CdTe due to the interfacial interaction between the K atoms layer and Te atoms layer. The upper panel in Fig. 5(b) shows the atomic stacking and charge transfer distribution in the planar view between mica and CdTe. The lower panel in Fig. 5(b) presents the cross section of the blue dashed line noted in the upper panel in Fig. 5(b). From Fig. 5(b) we could observe the strong electronic interaction between K atoms layer of mica and Te atoms layer of CdTe.

The characteristics of the interfacial interactions between the mica and CdTe are then determined by estimating the contribution of vdW interaction through comparing the difference between interaction energies of the nonlocal correlation functional and the one without it [36]. In the two sequential calculations, we first calculated the interfacial characteristics including the nonlocal vdW interactions with the optB86b-vdW functional, shown as the red column in Fig. 5(c). Then, utilizing the same atomic structure, we calculated the interfacial properties of the mica/CdTe with only the plain PBE and obtained the blue column in Fig. 5(c). Comparing the two columns, we could distinguish the energy scale of vdW interaction. The obtained results in Fig. 5(c) indicate that the contribution of vdW interaction is about 20%, while 80% of interfacial energy arises from the interaction between the K atoms layer in mica and Te atoms layer in CdTe. This finding is in contrast to the common belief that epitaxial film growth on mica is mainly through van der Waals interactions [9]. However, the result is consistent with a recent study of a soft perovskite material on mica where an ionic interaction between $CsPbBr_3$ and mica was shown to play an important role in the epitaxial growth of the film [37]. This stronger interface chemical interaction on mica compared to the traditional van der Waals interaction may explain the smaller angular orientational dispersion of CdTe on mica as compared to that on graphene (a vdW interaction dominating interface) [12].

G. Optical measurements

Figure 6(a) shows room temperature Raman spectra of the CdTe film grown on mica at 450 °C measured under 514 and 785 nm excitation wavelengths. For 785 nm excitation, five longitudinal optical (LO) peaks (LO, 2LO, 3LO, 4LO, and 5LO) are present in the Raman spectrum (black curve). The background hump in the spectrum comes from the resonant Raman scattering, or the so-called photoluminescence (PL) band edge emission. After background removal and peak fit, the peak positions and FWHMs (in the parentheses) for LO, 2LO, 3LO, 4LO, and 5LO in Fig. 6(a) are determined to be 168 (13.5), 336 (21.7), 505 (34.7), 670 (26.7), and 835 (50.3) cm^{-1}, respectively. The FWHMs of Raman LO peaks overall increase as the mode order increases. It can be explained through the energy and time uncertainty relationship or $\Delta E \Delta t \sim h/2\pi$, where h is the Planck constant

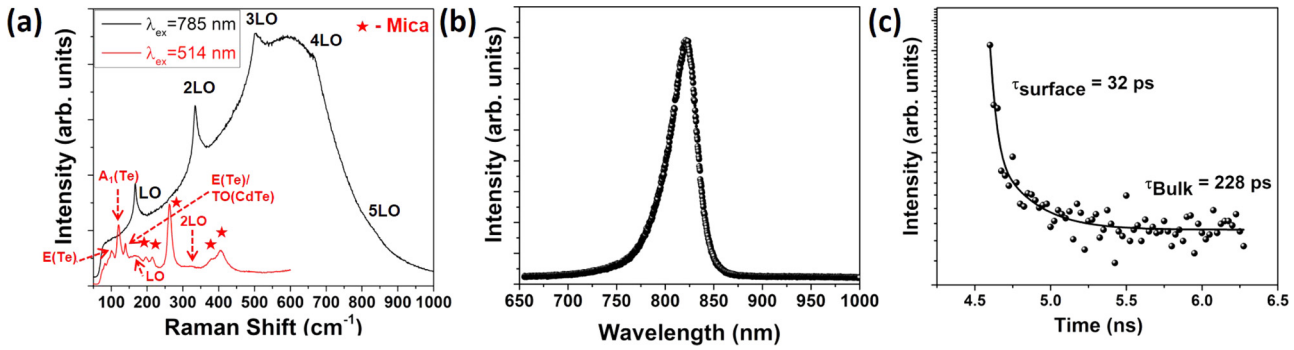

FIG. 6. (a) Room temperature Raman spectra of the CdTe film grown on mica at 450 °C with excitation wavelengths of 514 nm (red curve) and 785 nm (black curve). The stars indicate the Raman peaks from mica. The Te/CdTe peaks indicated by red arrows are listed in Table II. (b) Room temperature PL spectrum of the CdTe film grown on mica at 450 °C using a 532 nm laser excitation. The CdTe PL peak is at 817.6 nm. (c) TRPL decay curve. The two-exponential fitted TRPL decay curve suggests the surface and bulk lifetimes to be $\tau_1 = 32$ ps and $\tau_2 = 228$ ps, respectively.

[38,39]. Briefly, ΔE is the energy spread of a phonon mode and is represented by the FWHM of a Raman peak and Δt is the lifetime of a phonon. As the mode goes higher, a phonon can find more pathways to relax and is thus characterized with a shorter lifetime. Hence, the increasing FWHM from LO to 5LO echoes with the decreasing phonon lifetime.

Raman spectrum obtained with a 514 nm excitation (red curve) shows four vibration modes E(Te), A_1(Te), E(Te)/TO(CdTe), and LO(CdTe). TO is an aberration for transverse optical. Table II lists the quantitative analysis of peak positions and FWHMs using this 514 nm excitation. The measured Raman peaks from bulk CdTe(111) film, 300 Å thick pure Te film, and bulk CdTe crystal reported in the literature are also listed in Table II for a comparison. Except the E(Te) and A_1(Te) modes that may originate from Te precipitates, the E(Te)/TO(CdTe) and LO(CdTe) modes are close to the modes measured from the bulk CdTe crystals [40,41]. These peak positions suggest that the local chemical elements of our CdTe are close to its stoichiometry. In the spectrum, mica peaks are labeled by stars. Peaks at 196.3, 263.2, and 406.5 cm^{-1} are consistent with a report in the literature, where a weak peak at 197 cm^{-1}, a strong peak at 263 cm^{-1}, and a medium peak at 407 cm^{-1} were measured from mica using the same 514-nm excitation wavelength [42]. If a 534-nm excitation wavelength is used, the peak positions are 191, 262, and 419 cm^{-1}. Singh *et al.* assigned these three peaks to be vibration mode from L(Al-OH), bending mode δ(O-Si-O), and bending mode δ(O-Al-O). These peak positions also show that the local chemical elements of mica are close to its stoichiometry. Similar Raman data can be found in Fig. S4 for the film grown at 250 °C [18].

Room temperature PL from the CdTe film grown at 450 °C shows a single peak in Fig. 6(b). Peak fit leads to a peak center at 817.6 nm and a FWHM of 37.7 nm. These numbers correspond to a band gap of 1.516 eV and a FWHM of 0.070 eV. For the 1.5–2-μm-thick CdTe film grown on polycrystalline graphene, the PL peak was located at 829 nm (1.495 eV) with a FWHM of 60 nm (or 0.108 eV) [12]. For CdTe powders, the measured PL peak was at 822 nm (1.508 eV) [17]. The time-resolved PL(TRPL) of the CdTe film grown at 450 °C on mica shows a decay function, shown in Fig. 6(c). A curve fit of the time decay by assuming time parameters τ_1 and τ_2 gives carrier lifetime $\tau_1 = 32$ ps near the surface and $\tau_2 = 228$ ps in the bulk. Both numbers are comparable to those of 1.5–2-μm-thick CdTe film on graphene [12], 2-μm and 500-nm thick CdTe films grown by MOCVD on CdS [19], and the reported value of $\tau_1 = 4$–90 ps and $\tau_2 = 470$–725 ps for untreated single crystal CdTe sample [43]. The as grown CdTe thin films usually exhibit very high surface recombination velocity ($\sim 10^5$–10^7 cm/s) limiting their measured minority carrier lifetime [44,45]. Furthermore, our CdTe film is only ~100 nm thick, and the typical laser penetration depth for a CdTe film is ~200 nm [46]. Hence, the surface is the major contributor towards the minority carrier lifetime in our film. For such a thin film, the high surface recombination may overshadow any improvement in lifetime associated with larger size grains [47].

III. EXPERIMENT

The CdTe films were grown on mica substrates (size ~2 cm × 3 cm) by MOCVD in a vertical, cold wall chamber [12]. A

TABLE II. Room temperature Raman peak positions and FWHMs of the CdTe film grown on mica at 450 °C, along with reported data from literature.

Samples	E(Te) (cm^{-1})	A_1(Te) (cm^{-1})	E(Te)/TO(CdTe) (cm^{-1})	LO(CdTe) (cm^{-1})	Source
CdTe(111) film	100.9 (6.6)	120.6 (9.7)	139.8 (6.4)	167.5 (31.5)	This work
Bulk CdTe(111)	–	127.5	140	167	Ref [41]
Te film 300 Å	92	121.5	141.5	–	Ref [41]
Bulk CdTe(110)	–	129	147	171	Ref [40]

3-inch rotating quartz substrate holder with heating capability was used to hold the substrates. The metalorganic precursors used for Cd and Te were dimethylcadmium (DMCd) (25 sccm of H_2 through the bubbler) and diisopropyltelluride (DIPTe) (110 sccm of H_2 through the bubbler), respectively. Hydrogen was the carrier gas and its flow rate through the chamber was maintained at 2200 sccm during the one-step growth process. Films were grown at 450 °C for 10 min and at 250 °C for 60 min. The total chamber pressure was 100 Torr. The mole fractions of DMCd and DIPTe were maintained at 1.1×10^{-4} and 9.7×10^{-5}, respectively. The SEM cross section images of the films show that the CdTe films' thicknesses are ∼100 nm for both 450 and 250 °C growth temperatures.

The surface morphologies of the CdTe films were imaged using an AFM (PSI XE100) in noncontact mode. The AFM tip (μmash, NSC16/F/AIBS) used had a tip radius of less than 10 nm, a force constant of 35 N/m, and a resonant frequency of 170 kHz. SEM images were taken on a Zeiss Supra 55 SEM using an electron beam energy of 1.5 keV and a 30 μm aperture. XRD scans and rocking curves were collected by a Bruker D8 Discover x-ray diffractometer (Cu Kα, λ = 1.5406 Å) and the step size used was 0.01°. A step size of 2° was used for both azimuthal angle ϕ and chi angle χ for the pole figure data collection. For azimuthal scans of {111} poles at a fixed chi angle the step size used was 0.1°. EBSD characterization was carried out with a Carl Zeiss Ultra 1540EsB SEM-FIB system integrated with a NordlysNano EBSD Detector (Oxford Instruments). EDS spectra were also collected using an X-Max silicon drift detector (Oxford Instruments) in the SEM-FIB system. For EBSD and EDS characterizations, a 20 kV electron beam was used. The sample was tilted at 70° relative to the electron beam, with a working distance of 18 mm. The scan area was set 8.0×8.0 μm with a scan step size of ∼100 nm. The crystallographic orientation data was collected by the Aztec EBSD data acquisition software and post-analyzed using the HKL Channel 5 software package (Oxford Instruments). A RHEED pattern was projected on a phosphor screen mounted on a 6-inch flange in a high vacuum chamber (10^{-8} Torr). The electron beam with 20 keV energy was generated from an electron gun (model RDA-003G) using an emission current of 48 μA. The electron beam stroke at a glancing angle of <1° on the sample surface and was perpendicular to the phosphor screen. The sample holder can be rotated azimuthally around an axis perpendicular to the sample surface with a step increment of 1.8° by a high vacuum compatible step motor. This allowed RHEED patterns to be collected at different azimuthal angles. The RHEED pattern on the phosphor screen was captured by a digital camera positioned outside the vacuum chamber. The scale bar in units of inverse angstrom was calibrated [8] using a RHEED pattern of a bulk single crystal CdTe film with a known lattice constant of 6.48 Å.

TEM analysis of the CdTe/mica sample was carried out in both cross-sectional and planar geometries. The TEM (JEOL JEM-2011) incident electron energy was 200 keV. The real space images of the samples were taken with magnifications ranging from 20,000X to 1,500,000X. All the diffraction patterns were obtained using the same camera length of 2 meters which was calibrated previously. The cross-sectional CdTe/mica sample was prepared in the Carl Zeiss Ultra 1540EsB SEM-FIB system integrated with a Kleindiek MM3A-EM micromanipulator. A TEM lamella with dimensions of ∼40 μm×10 μm and a thickness of ∼2 μm was first cut out from the bulk sample using a 30 KeV gallium ion beam. It was then *in situ* lifted out using the micromanipulator equipped with a tungsten probe tip and attached to a copper PELCO FIB lift-out TEM grid. The attached lamella was further thinned down to ∼100-200 nm for TEM characterization. The planar TEM sample was prepared by first peeling off the CdTe thin film together with a few layers of mica using a scotch tape. The scotch tape with the sample beneath was then stuck to a silicon wafer. The sample was then heated to ∼100 °C and immersed in acetone in order to remove the scorch tape but retain the CdTe/mica sample on the silicon wafer. Finally, a lacey carbon TEM grid was physically attached to the silicon wafer to transfer part of the CdTe/mica sample to the grid. The transferred sample on the grid was electron transparent for planar characterization.

Raman spectroscopy (Renishaw model 2000 A) was conducted in back-scattering mode at room temperature. Two excitation wavelengths, 514 nm and 785 nm were used. The laser spot was ∼5.0 μm in size. Typically, the measurements were conducted with an integration time of 10 s and an accumulation of five spectra. PL was measured with a home-built confocal microscope setup, with a 532 nm CW laser as the excitation. A spectrograph (Andor) and a thermoelectric cooled CCD camera (Andor) was used for the spectroscopy. The TRPL was measured through the time-correlated single photon counting technique, and an avalanche photodiode detector (PDM series, Micro Photon Devices) was used. A pulsed laser centered at 532 nm was used as the excitation source. For both PL and TRPL measurements, the laser power was 200 μW with a beam diameter of 2 μm.

IV. CONCLUSION

We present epitaxial growth of ∼100 nm single crystalline CdTe films, in multilevel island format, on ∼13% lattice mismatched mica using MOCVD. The epitaxial relationship of CdTe with respect to mica is revealed by several diffraction-based techniques as follows: out-of-plane CdTe(111)//mica(001) and in-plane CdTe [$\bar{1}2\bar{1}$]//mica [010] and CdTe [$10\bar{1}$]//mica [100]. The texture of CdTe thin films is coherent from CdTe/mica interface to CdTe bulk and surface. For the film grown at 450 °C, x-ray characterization reveals very small orientation dispersions along out-of-plane and in-plane directions. EBSD IPF-Z mapping indicates that the grain sizes are tens of μm and, if the twin boundaries are excluded, larger than 250 μm. First-principles DFT calculations indicate that in addition to the known van der Waals interaction at the CdTe/mica interface, there is a large contribution (80%) in the interfacial energy due to chemical interactions, which may explain the unusually high epitaxial quality of the film compared to the films grown on pure van der Waals surfaces such as graphene. The results in this work may lead to potential flexible optoelectronic device applications that are not available presently.

ACKNOWLEDGMENTS

This experimental work was supported by the NSF Awards No. DMR-1305293 and No. CMMI–1635520, the New York State Foundation of Science, Technology and Innovation (NYSTAR) through Focus Center-New York C150117, and RPI Presidential fellowship (Y.X., Y.W.). The DFT calculations were supported by the National Natural Science Foundation of China (Grants No. 51705017 and No. U1706221).

[1] J. Yin, Q. Huang, and J. Zhou, Mechanism of different orientaion of CdTe on GaAs by molecular beam epitaxy, J. Appl. Phys. **79**, 3714 (1996).

[2] J. M. Ballingall, W. J. Takei, and B. J. Feldman, Low defect density CdTe(111)-GaAs(001) heterostructures by molecular beam epitaxy, Appl. Phys. Lett. **47**, 599 (1985).

[3] N. Matsumura, T. Ohshima, J. Saraie, and Y. Yodogawa, Preparation of CdTe thin films on Ge substrates by molecular beam epitaxy, J. Cryst. Growth **71**, 361 (1985).

[4] M. I. Abdalla and D. B. Holt, The epitaxial growth and strucutre of films of CeTe evaporated onto Ge, Phys. Stat. Sol. (a) **17**, 267 (1973).

[5] K. Lischka, E. J. Fantner, T. W. Ryan, and H Sitter, X-ray rocking curves from (100) and (111) CdTe grown on (100) GaAs by hot wall epitaxy, Appl. Phys. Lett. **55**, 1309 (1989).

[6] Q. Jiang, A. W. Brinkman, B. J. Cantwell, J. T. Mullins, F. Dierre, A. Basu, P. Veeramani, and P. Sellin, Growth of thick epitaxial CdTe films by close space sublimation, J. Electron. Mater. **38**, 1548 (2009).

[7] S. Neretina, R. A. Hughes, N. V. Sochinskii, M. Weber, K. G. Lynn, J. Wojcik, G. N. Pearson, J. S. Preston, and P. Mascher, Growth of CdTe/Si(100) thin films by pulsed laser deposition for photonic applications, J. Vac. Sci. Technol. **24**, 606 (2006).

[8] L. Chen, J. Dash, P. Su, C. F. Lin, I. Bhat, T.-M. Lu, and G.-C. Wang, Instrument response of reflection high energy electron diffraction pole figure, Appl. Surf. Sci. **288**, 458 (2014).

[9] M. I. B. Utama, Q. Zhang, J. Zhang, Y. Yuan, F. J. Belarre, J. Arbiol, and Q. Xiong, Recent developments and future directions in the growth of nanostructures by van der Waals epitaxy, Nanoscale **5**, 3570 (2013).

[10] A. Koma, Van der Waals epitaxy—a new epitaxial growth method for a highly lattice-mismatched system, Thin Solid Films **216**, 72 (1992).

[11] Y. Jung, G. Yang, S. Chun, D. Kim, and J. Kim, Growth of CdTe thin films on graphene by close-spaced sublimation method, Appl. Phys. Lett. **103**, 231910 (2013).

[12] D. Mohanty, W. Xie, Y. Wang, Z. Lu, J. Shi, S. Zhang, G.-C. Wang, T.-M. Lu, and I. B. Bhat, van der Waals epitaxy of CdTe thin film on graphene, Appl. Phys. Lett. **109**, 143109-1 (2016).

[13] W. de Poel, S. Pintea, J. Drnec, F. Carla, R. Felici, P. Mulder, J. A. A. W. Elemans, W. J. P. van Enckevort, A. E. Rowan, and E. Vlieg, Muscovite mica: Flatter than a pancake, Surf. Sci. **619**, 19 (2014).

[14] H. Poppa and A. G. Elliot, The surface composition of mica substrates, Surf. Sci. **24**, 149 (1971).

[15] D. Ma, J. Shi, Q. Ji, K. Chen, J. Yin, Y. Lin, Y. Zhang, M. Liu, Q. Feng, X. Song, X. Guo, J. Zhang, Y. Zhang, and Z. Liu, A universal etching-free transfer of MoS2 films for applications in photodetectors, Nano Res. **8**, 3662 (2015).

[16] B. R. Kumar, B. Hymanvathi, and T. S. Rao, Studies on optoelectronic properties of DC reactive magnetron sputtered CdTe thin films, AIP Conf. Proc. **1576**, 73 (2014).

[17] R. Cheng, Y. Wen, L. Yin, F. Wang, F. Wang, K. Liu, T. A. Shifa, J. Li, C. Jiang, Z. Wang, and J. He, Ultrathin single-crystalline CdTe nanosheets realized via Van der Waals epitaxy, Adv. Mater. **29**, 1703122 (2017).

[18] See Supplemental Material at http://link.aps.org/supplemental/10.1103/PhysRevMaterials.2.113402 for experimental data of the CdTe film grown at 250 Celsius degree.

[19] Y. B. Yang, L. Seewald, D. Mohanty, Y. Wang, L. H. Zhang, K. Kisslinger, W. Xie, J. Shi, I. Bhat, S. Zhang, T.-M. Lu, and G.-C. Wang, Surface and interface of epitaxial CdTe film on CdS buffered van der Waals mica substrate, Appl. Surf. Sci. **413**, 219 (2017).

[20] R. L. Schwoebel, Step motion on crystal surfaces. II. J. Appl. Phys. **40**, 614 (1969).

[21] R. L. Schwoebel and E. J. Shipsey, Step motion on crystal surfaces, J. Appl. Phys. **37**, 3682 (1966).

[22] G. Ehrlich and F. G. Hudda, Atomic view of surface self-diffusion: Tungsten on Tungsten, J. Chem. Phys. **44**, 1039 (1966).

[23] S. J. Liu, H. Huang, and C. H. Woo, Schwoebel-Ehrlich barrier: from two to three dimensions, Appl. Phys. Lett. **80**, 3295 (2002).

[24] X. Yin, J. Shi, X. Niu, H. Huang, and X. Wang, Wedding cake growth mechanism in one-dimensional and two-dimensional nanostructure evolution, Nano Lett. **15**, 7766 (2015).

[25] A. P. Belyaev, V. P. Rubets, and I. P. Kalinkin, Initial stages in the formation of epitaxial films of II–VI compounds on a muscovite mica substrate under highly nonequilibrium conditions, Phys. Solid State **39**, 333 (1997).

[26] J. L. Reno, P. L. Gourley, G. Monfroy, and J. P. Faurie, Effects of substrate misorientation on the structural properties of CdTe(111) grown by molecular beam epitaxy on GaAs(100), Appl. Phys. Lett. **53**, 1747 (1988).

[27] J.-S. Park, J. Kang, J.-H. Yang, W. Metzger, and S.-H. Wei, Stability and electronic structure of the low-sigma grain boundaries in CdTe: a density functional study, New J. Phys. **17**, 013027 (2015).

[28] F. Tang, T. Parker, G.-C. Wang, and T.-M. Lu, Surface texture evolution of polycrystalline and nanostructured films: RHEED surface pole figure analysis, J. Phys. D Appl. Phys. **40**, R427(R) (2007).

[29] Y. Alaskar, S. Arafin, D. Wickramaratne, M. A. Zurbuchen, L. He, J. McKay, Q. Lin, M. S. Goorsky, R. K. Lake, and K. L. Wang, Towards van der Waals epitaxial growth of GaAs on Si using a graphene buffer layer, Adv. Funct. Mater. **24**, 6629 (2014).

[30] G. Kresse and J. Furthmüller, Efficient iterative schemes for ab initio total-energy calculations using a plane-wave basis set, Phys. Rev. B **54**, 11169 (1996).

[31] P. E. Blöchl, Projector augmented-wave method, Phys. Rev. B **50**, 17953 (1994).

[32] J. P. Perdew, K. Burke, and M. Ernzerhof, Generalized Gradient Approximation Made Simple , Phys. Rev. Lett. **77**, 3865 (1996).

[33] J. Klimeš, D. R. Bowler, and A. Michaelides, Chemical accuracy for the van der Waals density functional, J. Phys.: Condens. Matter **22**, 022201 (2009).

[34] J. Klimeš, D. R. Bowler, and A. Michaelides, Van der Waals density functionals applied to solids, Phys. Rev. B **83**, 195131 (2011).

[35] T. Björkman, Testing several recent van der Waals density functionals for layered structures, J. Chem. Phys. **141**, 074708 (2014).

[36] A. N. Rudenko, F. J. Keil, M. I. Katsnelson, and A. I. Lichtenstein, Graphene adhesion on mica: Role of surface morphology, Phys. Rev. B **83**, 045409 (2011).

[37] Y. Wang, L. Gao, Y. Yang, Y. Xiang, Z. Chen, Y. Dong, H. Zhou, Z. Cai, G.-C. Wang, and J. Shi, Nontrivial strength of van der Waals epitaxial interaction in soft perovskites, Phys. Rev. Mater. **2**, 076002 (2018).

[38] H. Gao, F. Yan, H. zhang, J. Li, J. Wang, and J. Yan, First and second order Raman scattering spectroscopy of nonpolar a-plane GaN, J. Appl. Phys. **101**, 103533 (2007).

[39] L. Bergman, D. Alexson, P. L. Murphy, R. J. Nemanich, M. Dutta, M. Stroscio, C. Balkas, H. Shin, and R. F. Davis, Raman analysis of phonon lifetimes in AlN and GaN of wurtzite, Phys. Rev. B **59**, 12977 (1999).

[40] S. S. Islam, S. Rath, K. P. Jain, and S. C. Abbi, Forbidden one-Lo-phonon resonant Raman scattering and multiphonon scattering in pure CdTe crystals, Phys. Rev. B **46**, 4982 (1992).

[41] P. M. Amirtharaj and F. H. Pollak, Raman scattering study of the properties and removal of excess Te on CdTe surfaces, Appl. Phys. Lett. **45**, 789 (1984).

[42] M. Singh and L. Singh, Vibrational spectroscopic study of muscovite and biotite layered phyllosilicates, Ind. J. Pure & Appl. Phys. **54**, 116 (2016).

[43] M. O. Reese, C. L. Perkins, J. M. Burst, S. Farrell, T. M. Barnes, S. W. Johnston, D. Kuciauskas, T. A. Gessert, and W. K. Metzger, Intrinsic surface passivation of CdTe, J. Appl. Phys. **118**, 155305 (2015).

[44] R. Cohen and V. Lyahovitskaya, Unusually low surface recombination and long bulk lifetime in n-CdTe single crystals, Appl. Phys. Lett. **73**, 1400 (1998).

[45] J. P. Ponpon, A review of ohmic and rectifying contacts on cadmium telluride, Solid State Electron. **28**, 689 (1985).

[46] D. E. Aspnes and H. Arwin, Nondestructive analysis of $Hg_{1-x}Cd_xTe$ ($x = 0.00$, 0.20, 0.29, and 1.00) by spectroscopic ellipsometry. I. Chemical oxidation and etching, J. Vac. Sci. Technol. A: Vac. Surf. Films **2**, 1309 (1984).

[47] S. A. Jensen, J. M. Burst, J. N. Duenow, H. L. Guthrey, J. Moseley, H. R. Moutinho, S. W. Johnston, A. Kanevce, M. M. Al-Jasim, and W. K. Metzger, Long carrier lifetimesin large-grainpolycrystallne CdTe without $CdCl_2$, Appl. Phys. Lett. **108**, 263903 (2016).